NUMERICAL INVESTIGATION OF AERODYNAMICS OF A HELICOPTER ARTICULATED MAIN ROTOR IN HOVERING AND HORIZONTAL FLIGHT

I. Abalakin, V. Bobkov, T. Kozubskaya, V. Tsvetkova

vbobkov@keldysh.ru, Keldysh Institute of Applied Mathematics, Russian Federation

V. Vershkov, B. Kritsky, R. Mirgazov

ruslan.mirgazov@tsagi.ru, Central Aerohydrodynamic Institute, Russian Federation

Abstract

The paper is devoted to the numerical study of aerodynamic characteristics of a four-bladed articulated main rotor of a helicopter with cyclic pitch control and flapping motions of the blades and to the comparative analysis of the results against the similar case of rigid rotor with the fixed pitch angle and precone angle. The numerical investigation is carried out for the following working conditions: hover mode without cyclic control; forward flight without cyclic control; forward flight with cyclic control. The computations are performed on unstructured hybrid meshes using the in-house CFD code NOISEtte.

1. INTRODUCTION

The aerodynamic characteristics of the helicopter main rotor is still a challenging task. Due to the constantly tightening requirements for the operation of helicopters in terms of passenger safety, economic efficiency and noise level, as well as the constantly increasing cruise flight speed of helicopters, it is necessary to study in more detail the features of the flow around each element of the aircraft in order to obtain and predict results with a higher accuracy. Preliminary numerical simulations of aircraft aerodynamic and acoustic characteristics allows to significantly reduce a number of variants of models of new rotor blades that need to be manufactured.

The vortex-based methods allow to evaluate the integral aerodynamics characteristics very fast, but only the computational fluid dynamics (CFD) methods allow to get the full picture of surface distributions and flow features. However, the blades movements like dynamic blade flapping, blade lead-lag and blade pitching make the simulation very complex and require specific techniques to take them into account.

There are three basic approaches to simulate the movement of complex solid surfaces within CFD: dynamic mesh reconstruction, mesh deformation and overset mesh (chimera). Each method has some pros and cons. There are very few research groups that can simulate the full articulated rotor dynamics using CFD approaches.

The rotor blade movement can be modelled in several ways. The simplest one is to use predefined movement laws. The more accurate approach is to combine CFD method with the analytically-prescribed blade movement model (like rotor trimming [1]). The next method is based on coupling the flow filed simulation with the rigid body motion theory.

The current work exploits the last approach. The mathematical model of flow near the rotating rotor is based on the unsteady Reynolds-averaged Navier-Stokes (URANS) equations. Then the pressure distribution on the blades surface obtained by the RANS-based CFD simulation is used to calculate the forces and predict the blades displacement in space. On the second stage, the blade movement is governed by solving the motion equations where the blade is represented by a set of point-masses.

The paper presents the results of applying this approach to the fully-articulated rotor in hover and in froward flight. The results of numerical simulation validated against the experimental data show that the blades motion significantly affect the rotor aerodynamics.

Th described approach is implemented as the

Presented at 47th European Rotorcraft Forum, United Kingdom, 7-9th September, 2021

module Flapping_Rotor within the in-house CFD code NOISEtte [2].

2. MATHEMATICAL MODEL

2.1. Basic equations

To simulate the external flow around the rotor with the rotational speed **ω**, the Reynolds-averaged Navier-Stokes (RANS) equations for compressible gas with the Spalart-Allmaras turbulence model are used. The equations system is considered in the non-inertial rotating reference frame [3].

2.2. Blades movement

The movement equations for a rigid blade in the flapping plane are solved in the module Flapping_Rotor specially intended for modelling the flapping motion. The blade is cutting on a finite number of elements with the point masses dm_i along the blade span. Then the moments equation in the swing plane relative to the horizontal hinge (HH) is written as:

$$F_{inertial} L_i = YL_i - dm_i g L_i \cos\beta - dm_i \omega^2 \left(L_i \cos\beta + \Delta x\right) L_i \sin\beta,$$

where $F_{inertial}$ is the resulting inertial force acting on the blade i-th element; L_i is the distance from the HH to the blade i-th element mass center; Y is the blade i-th element aerodynamic lifting force; g is the gravity acceleration; β is the blade flapping angle; ω is the rotor angular speed; Δx is the distance from the rotor axis of rotation to the HH. Then the equation of the blade dynamics in the flapping plane is written as:

$$\ddot{\beta} \sum_i dm_i \left(L_i + \Delta x\right)^2 = \sum_i F_{inertial} L_i \ .$$

This equation defines the blade angular acceleration $\ddot{\beta}$ at the current time t_2. Then this value is substituted into the formula that determines the blade deflection angle at the current time t_2, at the given values of the angular velocity $\dot{\beta}^{t_1}$ and the current blade flapping angle β^{t_1} at the time t_1:

$$\beta^{t_2} = \beta^{t_1} + \dot{\beta}^{t_1}\left(t_2 - t_1\right) + 0,5\ddot{\beta}\left(t_2 - t_1\right)^2 .$$

The forces acting on a point mass in the swing plane are considered when describing the motion equation of a rigid blade relative to a vertical hinge.

The formula for the blade collective pitch and the law of cyclic pitch control is written as:

$$\varphi^{t_2} = \varphi_0 + a_{1\varphi} \sin\psi + b_{1\varphi} \cos\psi - k_\varphi \beta.$$

Here φ^{t_2} is the angle of the blade installation at time t_2; φ_0 is the collective pitch angle; $a_{1\varphi}$, $b_{1\varphi}$ are the the first order Fourier coefficients of the sine and cosine harmonics; k_φ is the flap compensator.

The rotor rotation is modeled by the movement of the nodes of the numerical mesh. This technique is described below in section 3.3.

3. COMPUTATIONAL SETUP

3.1. Numerical method for simulating the near flow field

The method for simulating the near flow field is based on the Navier-Stokes equations considered in the rotating non-inertial reference frame. The space approximation is built in the vertex-centered framework when the variables are defined in the hybrid mesh vertices. According to the finite-volume approach, the conservation laws are formulated for the dual cells, i.e. the control volumes specially built around the vertices. The numerical flux through the dual cell faces is calculated by the Roe approximate Riemann solver. The higher accuracy of the numerical scheme is achieved thanks to the quasi-1D edge-oriented reconstructions of variables involved in the flux calculation. The resulting EBR (Edge Based Reconstruction) scheme is described in detail in [4-6].

To approximate the viscous terms of Navier-Stokes equations, we use the Galerkin method with linear basic functions.

The implicit three-layer second-order scheme with the Newton linearization is used for the time integration. At each Newton iteration, the resulting system of linear equations is solved by the stabilized bi-conjugate gradient (BiCGStab) method.

The mentioned numerical algorithms are implemented in the in-house code NOISEtte [2].

3.2. Boundary conditions

In all the simulations, on the rotor surface, the no-slip boundary conditions are used taking into account the surface rotational velocity within rotating frame of reference.

Since the numerical simulation is performed in a bounded region, some artificial boundary conditions must be imposed on the boundary of computational domain.

These boundary conditions are determined by splitting the fluxes relating the values of the gasdynamic parameters within the computation domain and their values in the distant flow in the directions of characteristic velocities. The latter values are determined by the characteristic relations for an isentropic gas [3].

3.3. Moving mesh

Let us give the formulation of the basic finite-volume scheme, which takes into account the movement of the nodes of the deformable mesh. It is formulated by accounting nodes and faces movement in discrete

conservation law for a control volume built around the mesh node.

Consider arbitrary Lagrangian Eulerian (ALE) formulation of the Navier–Stokes system of equations in a discrete form for the control volume K_i built around the mesh node i as part of a vertex-centered formulation

$$\int_{K_i} \frac{d\mathbf{Q}}{dt} dV + \int_{\partial K_i} \left(\mathbf{F}^C(\mathbf{Q}) - \mathbf{v}\mathbf{Q} \right) \cdot \mathbf{n}\, dS = \int_{K_i} \mathbf{S}(\mathbf{Q}, \nabla\mathbf{Q}) dV,$$

where ∂K_i is the boundary of the control volume (or cell), $\mathbf{n}$ is the unit external normal to the boundary ∂K_i and $\mathbf{v}$ is the velocity vector of the movement of the boundary. The numerical scheme of the finite volume method is constructed as

$$\frac{d\mathbf{Q}_i}{dt} = -\frac{1}{|K_i|} \sum_{j \in N_1(i)} \mathbf{h}_{ij} + S\left(\mathbf{Q}_i, (\nabla\mathbf{Q})_i\right),$$

$$\mathbf{h}_{ij} = \mathbf{h}_{ij}^{\,C} + \mathbf{h}_{ij}^{\,D},$$

where $|K_i|$ is the cell K_i volume, $N_1(i)$ is the set of mesh nodes adjacent to node i, h_{ij} is the numerical flow approximating the physical flow at the boundary between nodes i and j consisting of an approximation of the convective and viscous flows $\boldsymbol{h}_{ij}^{C}$ and $\boldsymbol{h}_{ij}^{D}$, respectively.

The approximation of the convective flux is constructed using on approximate method for solving the Riemann problem. In this work, the Roe method is used, in which the numerical convective flux can be represented as the sum of two terms corresponding to the central-difference and upwind approximations responsible for the transport and dissipation, respectively:

$$\boldsymbol{h}_{ij}(t) = \left[\frac{\mathbf{F}(\mathbf{Q}_i) + \mathbf{F}(\mathbf{Q}_j)}{2} \cdot \frac{\mathbf{n}_{ij}}{|\mathbf{n}_{ij}|} - \mathrm{v}_{ij} \frac{\mathbf{Q}_i + \mathbf{Q}_j}{2} \right]$$

$$-\delta \left[\frac{1}{2} \mathbf{S} \left| \mathbf{\Lambda} - \mathrm{v}_{ij} \mathbf{I} \right| \mathbf{S}^{-1} \left(\mathbf{Q}_j - \mathbf{Q}_i \right) \right],$$

$$\mathbf{n}_{ij} = \int_{\partial K_i(t) \cap \partial K_j(t)} \mathbf{n}\, dS,$$

$$\mathrm{v}_{ij}(t) = \frac{1}{|\mathbf{n}_{ij}|} \int_{\partial K_i(t) \cap \partial K_j(t)} \mathbf{v} \cdot \mathbf{n}\, dS,$$

where $\mathbf{\Lambda}_{ij}$ and $\mathbf{S}$ is a diagonal Jacobian eigenvalue matrix and eigenvector matrix respectively:

$$\mathbf{S}\mathbf{\Lambda}\mathbf{S}^{-1} = \frac{d\mathbf{F}}{d\mathbf{Q}}\left(\mathbf{Q}_{ij}\right) \cdot \frac{\mathbf{n}_{ij}}{|\mathbf{n}_{ij}|}$$

The detailed method description is given in [7].

3.4. Mesh deformation

The numerical algorithm for moving-mesh deformation with preserving the mesh topology is designed for modeling the deflection and rotation of the blade relative to the hinges located at one point offset from the axis of rotation of the main rotor. To do this, the entire computational domain is decomposed into three subdomains: external, buffer and internal zones (Fig. 1).

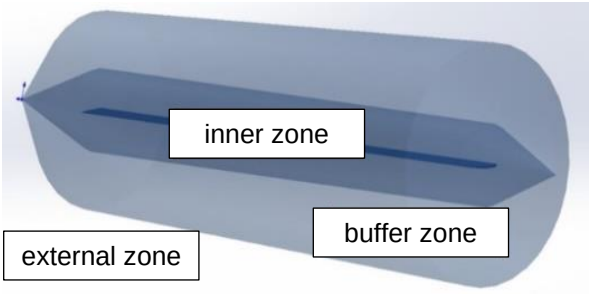

Fig.1. Mesh deformation zones

The inner area is built around the blade, the buffer zone is built around the inner zone with a certain indentation. The rest of the computational domain is considered as an external zone. For simplicity of constructing the deformation zones, the inner and buffer regions are analytically specified by the truncated cones, on the bases of which the cones are constructed. Such forms of the deformation zone are obtained due to the analytical piecewise linear weight function $f(\mathbf{r}_i)$, determined before the computation and specifying the amplitude of the node movement. In 3D, the function $f(\mathbf{r}_i)$ is defined as

$$f_x(x) = \begin{cases} \dfrac{x}{dx}, \text{ at } 0 \le x < dx \\ 1, \text{ at } dx \le x \le L_{blade} \\ \dfrac{dx_1 + L_{blade} - x}{dx_1}, \text{ at } L_{blade} < x \le L_{blade} + dx_1 \end{cases};$$

$$f_{rad}(\mathbf{r}_i) = \begin{cases} 1, \text{ at } 0 \le \alpha < R_{1z}(x) \\ \dfrac{R_{2z}(x) - \alpha}{R_{2z}(x) - R_{1z}(x)}, \text{ at } R_{1z}(x) \le \alpha \le R_{2z}(x); \\ 0, \text{ at } \alpha > R_{2z}(x) \end{cases}$$

$$\alpha = \sqrt{(c \cdot y)^2 + z^2}\,; \quad f(\mathbf{r}_i) = f_{rad}(\mathbf{r}_i) \cdot f_x(x).$$

Here $R_{1z}(x)$, $R_{2z}(x)$ are the analytical curves describing the boundaries of the inner and outer zones; x, y, z are the coordinates of the mesh node; L_{blade} is the blade length; dx is the distance from the hinge to the beginning of the feathered part of the blade; c is the control coefficient taken as 1. With this distribution, the weight function $f(\mathbf{r}_i)$ takes the value 1 at the boundary of the inner region and decreases with increasing the distance from the point $(x, 0, 0)$ to 0 at the boundary of the outer region.

The radius vector of the node *i* of the mesh at the time step *n+1* is evaluated as $\boldsymbol{r}_i^{n+1} = \boldsymbol{AB}\,\boldsymbol{r}_i^0$, where $\boldsymbol{A}$ is the rotation matrix by the angle ψ, $\boldsymbol{B}$ is the rotation matrix by the angles $f(\mathbf{r}_i)\beta$, $f(\mathbf{r}_i)\xi$ and $f(\mathbf{r}_i)\varphi$, $\mathbf{r}_i^0$ is the radius-vector of the node at time *t=0*.

Thus, all the nodes of the numerical mesh are rotated as a single unit by the angle ψ, simulating the rotation of main rotor. The nodes from the inner region move like a solid body, simulating the flap, swing movements and cyclic pitch control of the main rotor blades. In the buffer region, there is a radial linear decrease in the amplitude of the deviation of the mesh nodes from their original position, in order to provide a smooth junction of the inner and outer zones while maintaining the quality of the numerical mesh.

4. PROBLEM FORMULATION

The simulated main rotor is four-bladed rigid main rotor. The blades are rectangular in planform with a NACA23012 airfoil shape with twist (Fig. 2). The blades have the chord of 0.16 m and the radius of the blade root is 2.442 m. The total blade pitch angle is 10.1° and 6° for hover and forward flight respectively. The initial precone angle is 5°. The rotor angle of attack in all simulations was zero.

The rotation velocity is set to 840 RPM corresponding to the blade tip speed V_{tip} is 215 m/s. The flow velocity for forward flight is 60 m/s. The free-stream parameters correspond to the standard conditions under which the temperature is 20° C, the density ρ_0 is 1.2051 kg/m^3, the dynamic viscosity μ_0 is 1.827×10^{-5} Pa·s. These parameters determine the Reynolds number $Re = \rho_0 V_{tip} b/\mu_0$ ≈2.7×10^6.

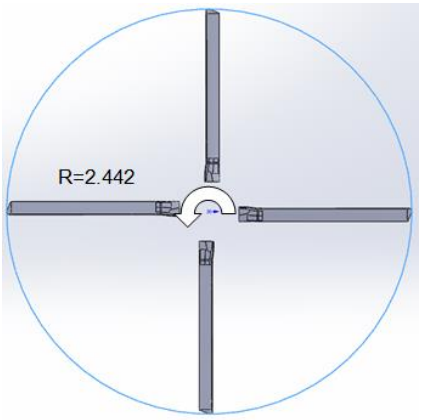

Fig.2. Simulated rotor geometry

The computational domain is filled with the mixed unstructured mesh refined in the regions where the detailed representation of flow structure is required. Thus, the finest mesh is built at the leading and trailing blade edges, at the blade tip. The blade surface is framed by the prismatic mesh layers with the exponentially increasing height. When the initially anisotropic prisms become close to isotropic, the mesh goes to a quasi-uniform tetrahedral unstructured form with a smooth coarsening towards the outer boundaries of computational domain.

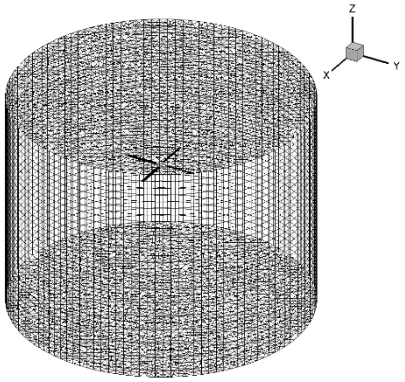

Fig.3. Computational mesh

The computational domain has a form of cylinder with the radius of 5 rotor radii (Fig. 3). The cylinder axis coincides with the helicopter rotation axis. The lower boundary of the computational domain is located at the distance of 5 rotor radii from the plane of rotation, and the upper boundary is at the distance of 3 radii. The resulting mesh consists of 8.3M nodes and 33M elements.

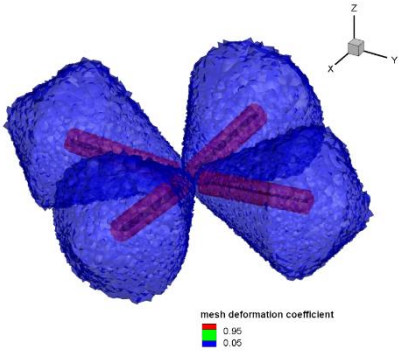

Fig.4. Deformation zones

The mesh “buffer” deformation zone (shown in blue color on the Fig.4) built around each blade occupies a small part of the entire computational domain. The mesh deformation laws in each sub-zone are set in accordance with the individual movements of each blade. At the interface between the deformable and non-deformable regions the conservation laws were satisfied. In all calculations, the main coordinate system was a right-handed Cartesian system with the Oz axis directed along the rotor rotation axis, and the Ox axis directed in the rotor rotation plane so that its positive projection coincided with the flow direction. The origin of coordinates coincided with the point of intersection of the axis of rotation and the plane of the rotor.

To evaluate the aerodynamic characteristics of the rotor with the given spatial motions, it was required to simulate up to 3 rotations of the rotor to attenuate the parasitic disturbances arising at the initial moment due to the mismatch of the flow fields and the motion of the rotor blades. Within simulation the 10 revolutions were performed in horizontal flight and 40 revolutions in hover. It is not enough for the starting vortex complete dissipate, but sufficient to move it downstream from the rotor blades and minimize its effect on the rotor aerodynamics.

5. RESULTS

5.1. Hovering rotor simulation

The goal of the first simulation was to investigate rotor aerodynamics with blades movements induced by aerodynamics forces as described in section 2.2 and compare numerical results with experimental data.

The numerical results for the case represented in the Table 1.

Tab. 1. Rotor aerodynamics in hover

	thrust, kgs	torque, kgs·m	β, °
numerical	793	189	4.5
experiment	811	180	3.2

The thrust and torque values are in good agreement with experiment meanwhile the flapping angle prediction is not so accurate.

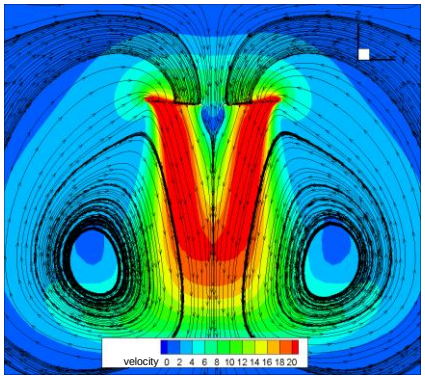

Fig.5. Velocity field and streamlines in hover

Figure 5 shows the velocity field and streamlines in cross-section view. Even after 40 rotor rotations simulation the starting vortex is still inside the calculation domain and it is affecting the flow induced by rotor downstream the rotor plane.

Figure 5 represents the turbulent structure of the flow visualized by Q-criterion iso-surfaces colored by the velocity magnitude. There is vortex wake downstream the rotor center, the tip vortex evolution resolved up to azimuth 270°.

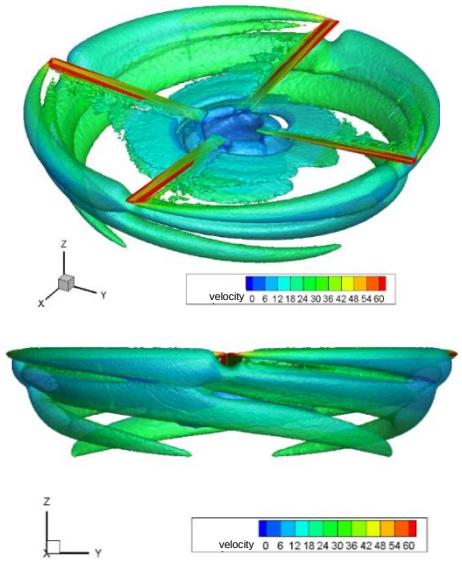

Fig.6. Q-criterion isosurface colored by velocity magnitude

5.2. Forward flight rotor simulation

In the next numerical experiment, the three types of blades motion of the rotor in forward flight were investigated and compared: the fully articulated rotor simulated with and without cyclic pitch control and rigid rotor simulation. The collective pitch was the same for all three cases.

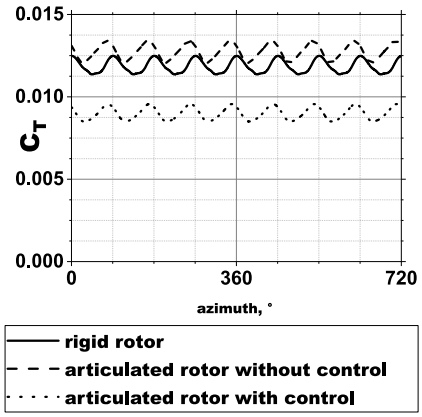

Fig.7. Thrust coefficient

Figures 7 and 8 represents the evolution of thrust and torque coefficients.

From these plots it is clearly seen that taking into account of cycling pitch control significantly decrease the torque coefficient oscillations amplitude and decreases thrust coefficient by 27%.

Thus, the cycling pitch control must be taken into account to perform accurate articulated rotor simulation.

Figures 9 and 10 shows the single blade thrust and whole rotor thrust evolution correspondingly. Figures

11 and 12 represents the blade cyclic pitch and flapping angle evolution. The evolution period on the plots 7-12 corresponds to two rotor rotations.

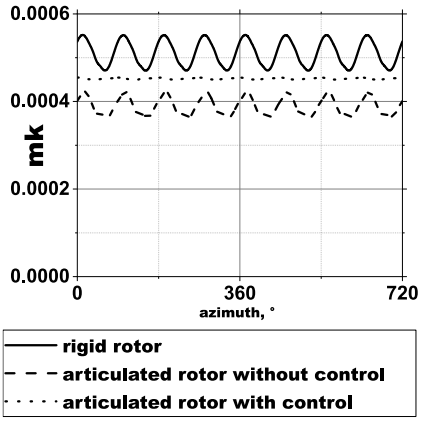

Fig.8. Torque coefficient

The thrust plots 9-10 demonstrates that flapping decreases single blade thrust oscillations amplitude meanwhile the total rotor thrust slightly increases and shift the thrust maximum azimuthal position.

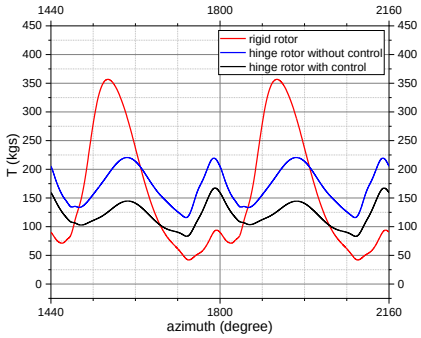

Fig.9. Single blade thrust evolution

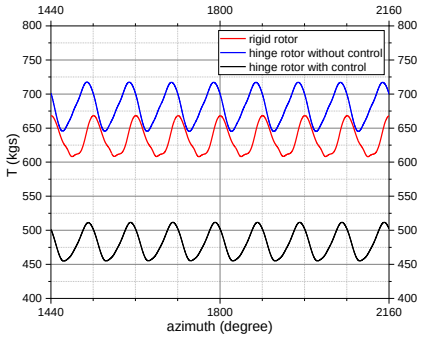

Fig.10. Rotor thrust evolution

From plots 11-12 it is seen that the cycling pith leads to rotor cone displacement and as result to blade angle of attack change. It leads to single blade thrust decrease by 50 kgs and rotor thrust decrease by 27%.

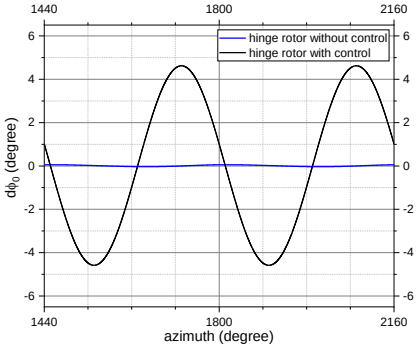

Fig.11. Cyclic pitch evolution

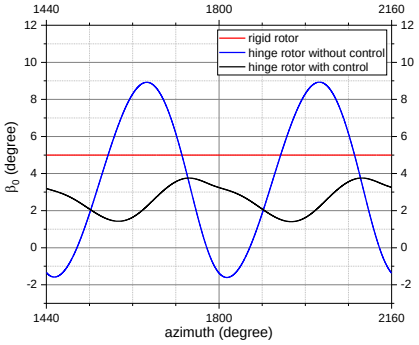

Fig.12. Flapping angle evolution

The turbulent structure visualized by Q-criterion iso-surfaces for values 1e-4, 1e-5, 1e-6 and colored by flow velocity magnitude presented on the Fig. 13-15.

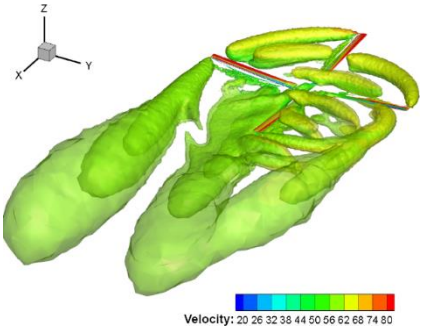

Fig.13. Turbulent structures near rigid rotor

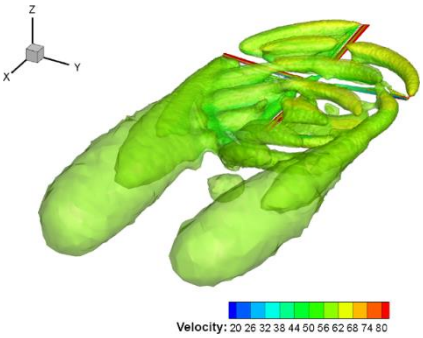

Fig.14. Turbulent structures near articulated rotor without cycling pitch control

It is noticeable that only in rigid rotor with cycling pitch control simulation the blades tip vortices are not interacts with blades and these structures moved downstream and lays below the rotor plane. It means that in simulation without cycling pitching control the blades load oscillations and acoustic field pulsations will be significantly higher.

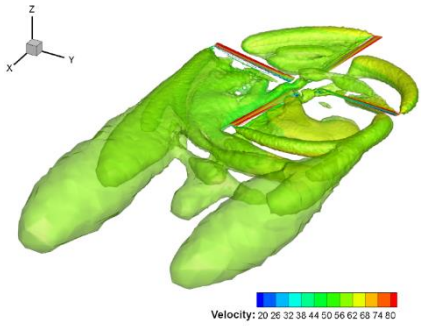

Fig.15. Turbulent structures near articulated rotor with cycling pitch control

6. CONCLUSION

The paper presents the results of numerical simulation of turbulent flow around the hinged articulated four-blades main rotor in hover and forward flight.

The numerical method is developed basing on the computational kernel of in-house code NOISEtte [2] by implementing the moving-mesh techniques and the efficient algorithm of mesh deformation to consider the cyclic pitch control and flapping motions of blades. The developed approach allows to simulate turbulent flow near a helicopter articulated rotor in real operating conditions in hover and forward flight modes.

The validation of the developed numerical method has been carried out by comparing with the available experimental data.

The results confirm that the cyclic pitch control and flapping blade motions significantly affect the flow field and rotor aerodynamics, and these motions must be taken into account in the case of articulated rotor CFD simulation.

This work has been carried out using computing resources of the federal collective usage center Complex for Simulation and Data Processing for Mega-science Facilities at NRC “Kurchatov Institute”, http://ckp.nrcki.ru/.

REFERENCES

1. Steijl R., Barakos G.N., Badcock K.J. A framework for CFD analysis of helicopter rotors in hover and forward flight // Int. J. Numer. Meth. Fluids. 2006. № 51. P. 819–847. DOI: 10.1002/fld.1086.
2. A.Gorobets. Parallel Algorithm of the NOISEtte Code for CFD and CAA Simulations // Lobachevskii Journal of Mathematics, 2018, V. 39, No. 4, P. 524–532. DOI: 10.1134/S1995080218040078
3. I. V. Abalakin, V. A. Anikin, P. A. Bakhvalov, V. G. Bobkov, and T. K. Kozubskaya. Numerical Investigation of the Aerodynamic and Acoustical Properties of a Shrouded Rotor // Fluid Dynamics, 2016, V. 51, No. 3, P. 419-433. DOI: 10.1134/S0015462816030145
4. Abalakin I., Bakhvalov P., Kozubskaya T. Edge-based reconstruction schemes for prediction of near field flow region in complex aeroacoustics problems // Int. J. Aeroacoust, 2014, V. 13, No. 3-4. P. 207-234. DOI: 10.1260/1475-472X.13.3-4.207
5. Abalakin I., Bakhvalov P., Kozubskaya T. Edge-based reconstruction schemes for unstructured tetrahedral meshes // Int. J. Numer. Meth. Fluids. 2016. V. 81, No. 6. P. 331-356. DOI: 10.1002/fld.4187
6. P. A. Bakhvalov. Quasi one-dimensional reconstruction scheme on convex polygonal meshes for solving aeroacoustics problems // Mathematical Models and Computer Simulations, 2016, V. 6, No. 2, P. 192-202. DOI: 10.1134/S2070048214020021
7. I. V. Abalakin, V. A. Vershkov, N. S. Zhdanova, T. K. Kozubskaya. Numerical simulation of acoustic fields induced by flow past oscillating solid // Mathematical Models and Computer Simulations, 2020, V. 12, No. 3, P. 422–432. DOI: 10.1134/S2070048220030023

Presented at 47th European Rotorcraft Forum, United Kingdom, 7-9th September, 2021